

A reference frame–based microgrid primary control for ensuring global convergence to a periodic orbit

Xinyuan Jiang^a, Constantino M. Lagoa^a, Daning Huang^b, Yan Li^{a,★}

^a*Department of Electrical Engineering, Pennsylvania State University, University Park, PA 16802, USA*

^b*Department of Aerospace Engineering, Pennsylvania State University, University Park, PA 16802, USA*

Abstract

Power systems with a high penetration of renewable generation are vulnerable to frequency oscillation and voltage instability. Traditionally, the stability of power systems is considered either in terms of local stability or as an angle oscillator synchronization problem with the simplifying assumption that the dynamics of the amplitudes are on much shorter time scales. Without this assumption, however, the steady state being studied is essentially a limit cycle with the convergence of its orbit in question. In this paper, we present a method to analyze the orbital stability of a microgrid and propose a voltage controller for the inverter-interfaced renewable generators. The main hurdle to the problem lies in the constant terms in the rotating internal reference frames of each generator. We extend the shifted passivity of port-Hamiltonian systems to the analysis of limit cycles and prove that, if the system is shifted passive without considering these constant terms, then the periodic orbit is globally attractive. To the best of our knowledge, this is the first global stability result for non-nominal steady states of the microgrid in the full state space, which provides new insights into the synchronization phenomenon where the dissipativity of the system ensures convergence. The proposed controller is verified with a test microgrid, demonstrating its stability and transient smoothness compared to the standard droop control.

Key words: Grid-forming control; Microgrid; Orbital stability; Equivariant system; Shifted passivity; Synchronization.

1 Introduction

Microgrids are considered key to achieving the sustainability of power systems in their transition from centralized generation to distributed energy resources (DER). Microgrid primary control refers to the lower-level control that defines the transient dynamics under sudden load or generation changes. Besides its steady-state characteristics, the primary control of the microgrid is designed to maintain stability under large power disturbances without relying on communication between DER units [22]. Hence, stability analysis of the microgrid primary control is the basis for microgrid functionalities, where the main problem is to find the optimal DER control scheme and parameters to ensure convergence of the overall microgrid to a steady state through a sufficiently

smooth transient.

A prerequisite for the primary control to maintain stability is to allow some flexibility in the DER power output, so that random power disturbances can be shared when steady state is reached. Steady-state power sharing is usually provided by the droop characteristic of the control (droop control), where active and reactive power outputs are lowered in response to the increases in voltage frequency and amplitude. Various implementations of droop control can be roughly divided into the swing equation [4, 20, 31, 32] and virtual oscillators [12, 18, 36]. In analyzing its stability, the variable steady-state frequency creates significant challenges, which can be explained by the synchronized steady state being a limit cycle [9, 44]. The frequency of the limit cycle is associated with the power sharing in the microgrid and is not fixed. Hence, the control objective is different from the usual a set point tracking problem as studied in [28, 35, 39].

The limit cycle steady state of the microgrid is related to the angle symmetry of the system, i.e., changing the angle reference leaves the dynamics unchanged. We refer to this type of steady state as a circular limit cycle

★ Corresponding author Y. Li. Tel. +1-814-863-9571. Fax +1-814-865-6392. This work was supported by Office of Naval Research under the award N00014-22-1-2504.

Email addresses: xuj49@psu.edu (Xinyuan Jiang), cml18@psu.edu (Constantino M. Lagoa), daning@psu.edu (Daning Huang), yq15925@psu.edu (Yan Li).

(Section 2). The usual approach to study the stability of circular limit cycles is to remove the symmetry by changing to transverse coordinates, i.e., replacing absolute angles by angle differences, and thereby reducing the limit cycle to an equilibrium point [2, 14, 29]. However, the following limitations exist with this approach:

- 1) In transverse coordinates, the sign-definite energy dissipation no longer stays sign-definite where it is mixed with the power sources. On the other hand, in the original coordinates, the power sources, once integrated, lead to monotonically decaying energy functions that are not lower bounded [4, 32]. As a compromise, the standard technique is to show that the unbounded energy function, having been transformed into transverse coordinates, is locally convex at the isolated equilibrium point in transverse coordinates [4, 32]. This certifies it as a local Lyapunov function. However, this technique cannot be used to obtain global stability results.
- 2) In transverse coordinates where the voltage angle dynamics are considered, the equilibrium points of the angle variables are isolated but repeat periodically in the space of \mathbb{R}^n . The fundamental problem is the periodicity of the original state space of \mathbb{T}^n [8]. This problem is overcome in [31], which first defines a Leonov function to bound the voltage angles in \mathbb{R}^n before applying the invariance principle to obtain the global convergence result.
- 3) Due to the complexities above, almost all existing studies only consider simplified models of the system, assuming time-scale separation. Attempts to amend these results to include the electromagnetic network dynamics lead to conservatism [36].

To date, few studies have addressed the stability of microgrids as the stability of a limit cycle (orbital stability) in the original coordinates. Some existing methods for studying orbital stability include Floquet theory and Poincaré map [25], method of slices [2], index iteration theory [5, 6], and transverse contraction [19]. Existing Lyapunov analyses of orbital stability rely on finding transverse and parallel coordinates [11, 19, 37, 44]. Other than transverse contraction, these methods suffer from the same issue with formulating dissipation in alternative coordinates, and transverse contraction may be too conservative for large-scale network systems. Recently, there have been several orbital stability studies for the dispatchable virtual oscillator control (dVOC). For example, [36] constructs a Lyapunov function for the full-order dynamics from that of the globally asymptotically stable reference dynamics by formalizing the time-scale separation assumption; [12] proposes a stability condition for a non-nominal steady state of dVOC such that the available dissipation in complex coordinates dominates the amplitude-regulating terms. Among these existing studies, an intrinsic approach to the orbital stability of microgrids in terms of the angle symmetry and the different reference frames from which the limit cycle

originates is still missing.

In this paper, we propose a primary DER control and a stability analysis for the non-nominal limit cycle steady states of the controlled microgrid. Firstly, the angle symmetry of the microgrid system is established. Then, the proposed control, which can be seen as a second-order integrator in the stationary reference frame, is presented. Assuming the existence of a circular limit cycle, we formulate the system as a port-Hamiltonian system with an artificial shrinking imposed on the solution sets. The latter allows us to decouple the voltage controller from the swing equation in the model. The energy balance of the shifted storage function is carefully derived so that the sign-indefinite terms related to the angle-dependent power sources are eliminated by shifting the phase of the steady state. Then, through analysis of the limiting solution, the circular periodic orbit of the microgrid is proved to be globally attractive under the shifted passivity condition. Finally, the control gain tuning is formulated based on the shifted passivity condition for DERs. The contributions are summarized as follows.

- A grid-forming DER control is proposed to ensure the global stability of the non-nominal microgrid steady states, independently of the parameters of the swing equation or the network topology that determine power sharing.
- The design of the DER control gain is formulated as a semidefinite program for each DER with only local parameters, which provides a distributed and robust stability guarantee for the whole microgrid.
- The concept of shifted passivity, suitable for verifying the stability of nonzero equilibrium points, is extended to the synchronization problem for phase oscillators with dynamic passive coupling, to connect passivity with the attractivity of the periodic orbit resulting from synchronization.

This paper is structured as follows. Basic definitions are given in Section 2. The model of the microgrid with the proposed control is presented in Section 3. The port-Hamiltonian model of the DER subsystem is constructed in Section 4, and the stability proof is presented in Section 5. The tuning of the control gain is in Section 6. Numerical example and conclusion are in Sections 7 and 8.

Notation. The imaginary unit is j . The matrix form of j is $\mathbf{J} = [0, -1; 1, 0]$. A zero vector is 0_n ; a vector of ones is 1_n ; an identity matrix is \mathbf{I}_n ; and a zero matrix is $\mathbf{0}_{n \times m}$. The standard basis for \mathbb{R}^n is $\{\mathbf{e}_1, \dots, \mathbf{e}_n\}$. For an $\mathbf{A} \in \mathbb{C}^{n \times n}$, the transpose is \mathbf{A}^\top , the Hermitian transpose is \mathbf{A}^* , the Moore-Penrose pseudoinverse is \mathbf{A}^\dagger , and the Hermitian part is $\text{He}\{\mathbf{A}\} = \frac{1}{2}(\mathbf{A} + \mathbf{A}^*)$. Denote by $\text{diag}(\mathbf{A}_1, \dots, \mathbf{A}_n)$ a block diagonal matrix with \mathbf{A}_i , $i = 1, \dots, n$ on the diagonal. Denote by $\text{col}(\mathbf{x}_i)$ a column vector that stacks the vectors \mathbf{x}_i , $i = 1, \dots, n$. The standard inner product for \mathbb{C}^n is $\langle \mathbf{y}, \mathbf{x} \rangle = \Re\{\mathbf{y}^* \mathbf{x}\}$.

For a Hermitian matrix \mathbf{A} , positive definiteness is denoted by $\mathbf{A} \succ 0$, i.e., $\langle \mathbf{x}, \mathbf{A}\mathbf{x} \rangle > 0$ for all $\mathbf{x} \in \mathbb{C}^n \neq 0_n$. For an $\mathbf{A} \succeq 0$, denote $\|\mathbf{x}\|_{\mathbf{A}}^2 = \langle \mathbf{x}, \mathbf{A}\mathbf{x} \rangle$. For a function $g : \mathbb{C}^n \rightarrow \mathbb{R}$ of complex variables, the complex gradient is $\nabla g(\mathbf{x}) = 2\text{col}(\frac{\partial g}{\partial x_i^*})$ where $\frac{\partial g}{\partial x_i^*}$ is the Wirtinger derivative [27]. Nominal set points for the control are denoted by $(\cdot)_{\text{nom}}$. The Kronecker product is \otimes .

2 Preliminaries

2.1 Symmetry and circular limit cycle

The circular limit cycle is defined in this subsection. A formal treatment of symmetries of ODEs can be found in Chapter 1 of [1]. The group characterization can be found in [15].

Definition 1 A one-parameter group is a differentiable homomorphism $\mathcal{T} : \mathbb{R} \rightarrow G$ from \mathbb{R} (additive group) to a topological group G such that $\mathcal{T}(\tau)\mathcal{T}(s) = \mathcal{T}(\tau + s)$. The infinitesimal generator of $\mathcal{T}(\tau)$ is $\mathcal{G} = \frac{\partial \mathcal{T}(\tau)}{\partial \tau} \Big|_{\tau=0}$.

Definition 2 For the system $\dot{\mathbf{x}} = \mathbf{f}(\mathbf{x})$ where $\mathbf{x} \in \mathbb{C}^n$, a continuous symmetry is a one-parameter group of automorphisms $\mathcal{T}(\tau) : \mathbb{C}^n \rightarrow \mathbb{C}^n$, such that each $\mathcal{T}(\tau)$ maps solutions of the system to solutions.

The microgrid system considered in this paper has the angle symmetry: $\mathcal{T}(\tau)\mathbf{x} = e^{j\tau}\mathbf{x}$. Since this $\mathcal{T}(\tau)$ is 2π -periodic in the parameter τ , τ naturally lives on the 1-torus $\mathbb{T} = \mathbb{R}/2\pi\mathbb{Z}$ with 2π equivalence [42].

Let us consider the implications of angle symmetry on the possible limiting solutions of the system.¹ For a given limiting solution $\bar{\mathbf{x}}(t)$, the following two scenarios exist:

- i) There is an $\bar{\omega} \in \mathbb{R} \neq 0$ such that $\dot{\bar{\mathbf{x}}}(t) = \bar{\omega}\mathcal{G}\bar{\mathbf{x}}(t) = j\bar{\omega}\bar{\mathbf{x}}(t)$ for all $t \in \mathbb{R}$. This is the case considered in this paper.
- ii) There is no such $\bar{\omega}$. The limit set is not isolated in this case according to Definition 2.

For i), the limiting solution is a limit cycle given by

$$\mathbf{x}(t) = e^{j\bar{\omega}t}\mathbf{x}(0), \quad (1)$$

where $\bar{\omega}$ is the frequency of the limit cycle. From Definition 2, mappings of $\mathbf{x}(t)$ in (1) by $\mathcal{T}(\tau)$ are also limit cycle solutions—with shifted phases. Let us designate one of these limit cycle solutions $\hat{\mathbf{x}}(t)$ to have phase 0; this set of limit cycle solutions can be denoted as

$$\bar{\mathbf{x}}(\tau, t) = \mathcal{T}(\tau)\hat{\mathbf{x}}(t),$$

¹ A limiting solution is a solution whose orbit is contained in a limit set [16].

for $\tau \in \mathbb{T}$, all of which share the circular orbit,

$$\text{span}(\bar{\mathbf{x}}(0, t)) = \{e^{j\tau}\hat{\mathbf{x}}(0) \mid \tau \in \mathbb{T}\}. \quad (2)$$

In the sequel, the time parameter in $\bar{\mathbf{x}}(\tau, t)$ is omitted, resulting in the notation $\bar{\mathbf{x}}(\tau)$ for a limit cycle solution of phase τ with the periodic orbit $\text{span}(\bar{\mathbf{x}}(\tau))$.

If $\bar{\omega} \neq 0$,² the limit cycle in scenario ii) is identified by the the following condition,

$$(\exists \mathbf{x} \in \mathbb{C}^n, \bar{\omega} \in \mathbb{R} \neq 0) \text{ s.t. } \mathbf{f}(e^{j\tau}\mathbf{x}) = j\bar{\omega}e^{j\tau}\mathbf{x}, \forall \tau \in \mathbb{T}. \quad (3)$$

Due to the additional parameter $\bar{\omega}$, the condition (3) for circular limit cycles is slightly harder to solve than the equilibrium point condition. To avoid this problem, it is commonplace in the literature to assume that $\bar{\omega}$ is equal to the nominal 60 (or 50) Hz. Then, in a reference frame rotating at frequency $\bar{\omega}$, the dynamics is transformed into $\dot{\mathbf{x}} = -j\bar{\omega}\mathbf{x} + \mathbf{f}(\mathbf{x})$, for which the equilibrium condition is solved. However, in practice, the steady-state frequency $\bar{\omega}$ is almost never equal to the nominal frequency due to the complex balance between power supply and demand [10]. In other words, an equilibrium point usually cannot be found in the nominal frequency reference for the precise model. This motivates the stability analysis for non-nominal limit cycles [12].

2.2 Shifted passivity of port-Hamiltonian system

The shifted passivity conditions proposed in [21] serve to characterize the passivity of port-Hamiltonian (pH) systems with respect to a nonzero equilibrium point. In this subsection, we introduce pH systems in the state space \mathbb{C}^n , which is a mild extension to the \mathbb{R}^n case in [40], and recall basic results on shifted passivity.

Consider a generic pH model for a subsystem of a network, of the form [40]

$$\dot{\mathbf{x}} = \mathbf{F}\nabla H(\mathbf{x}) + \mathbf{G}\mathbf{u} \quad (4a)$$

$$\mathbf{y} = \mathbf{G}^*\nabla H(\mathbf{x}), \quad (4b)$$

where $\mathbf{x} \in \mathbb{C}^n$ is the state vector, $H : \mathbb{C}^n \rightarrow \mathbb{R}_{\geq 0}$ is the Hamiltonian, $\mathbf{F} \in \mathbb{C}^{n \times n}$ is the system matrix, and $\mathbf{G} = [\mathbf{G}_1, \mathbf{G}_2]$ is the input matrix. The input $\mathbf{u} = [\mathbf{u}_1^T, \mathbf{u}_2^T]^T$ and output $\mathbf{y} = [\mathbf{y}_1^T, \mathbf{y}_2^T]^T$ are grouped as follows:

- 1) $(\mathbf{u}_1, \mathbf{y}_1)$ represents interactions within a microgrid network system being studied,
- 2) $(\mathbf{u}_2, \mathbf{y}_2)$ represents external disturbances such as load and mechanical input.

² The degenerate case $\bar{\omega} = 0$ can be removed by changing to a reference frame rotating at some nonzero frequency.

We denote by $\Omega \ni (\mathbf{x}(t), \mathbf{u}(t), \mathbf{y}(t))$ the solution set of the pH system (4) for any input function $\mathbf{u}(t)$.

For a continuously differentiable function $H : \mathbb{C}^n \rightarrow \mathbb{R}$, let us define the shifted version of $H(\mathbf{x})$ centered at an $\bar{\mathbf{x}} \in \mathbb{C}^n$ as

$$\mathcal{H}(\mathbf{x}, \bar{\mathbf{x}}) = H(\mathbf{x}) - H(\bar{\mathbf{x}}) - \langle \nabla H(\bar{\mathbf{x}}), \mathbf{x} - \bar{\mathbf{x}} \rangle, \quad (5)$$

which is the storage function for verifying shifted passivity [4, 21]. Its gradient w.r.t. \mathbf{x} is

$$\nabla_{\mathbf{x}} \mathcal{H}(\mathbf{x}, \bar{\mathbf{x}}) = \nabla H(\mathbf{x}) - \nabla H(\bar{\mathbf{x}}). \quad (6)$$

Claim: If $H(\mathbf{x})$ is quadratic, i.e., $H(\mathbf{x}) = \frac{1}{2} \langle \mathbf{x}, \mathbf{Q}\mathbf{x} \rangle$ for some $\mathbf{Q} = \mathbf{Q}^*$, then

$$\nabla_{\bar{\mathbf{x}}} \mathcal{H}(\mathbf{x}, \bar{\mathbf{x}}) = -\nabla_{\mathbf{x}} \mathcal{H}(\mathbf{x}, \bar{\mathbf{x}}). \quad (7)$$

From (5), we get $\mathcal{H}(\mathbf{x}, \bar{\mathbf{x}}) = \frac{1}{2} \langle \mathbf{x} - \bar{\mathbf{x}}, \mathbf{Q}(\mathbf{x} - \bar{\mathbf{x}}) \rangle$. Since $\mathcal{H}(\mathbf{x}, \bar{\mathbf{x}})$ is a function of $\mathbf{x} - \bar{\mathbf{x}}$, we obtain (7).

Definition 3 Consider the pH system (4) and an equilibrium point $(\bar{\mathbf{x}}, \bar{\mathbf{u}})$. Let $\bar{\mathbf{y}} = \mathbf{G}^* \bar{\mathbf{u}}$. The pH system is said to be shifted passive w.r.t. $(\bar{\mathbf{x}}, \bar{\mathbf{u}})$ if, for all \mathbf{x} , it holds that

$$\dot{\mathcal{H}}(\mathbf{x}, \bar{\mathbf{x}}) \leq \langle \mathbf{y} - \bar{\mathbf{y}}, \mathbf{u} - \bar{\mathbf{u}} \rangle.$$

To interpret Definition 3, let us write the energy balance as

$$\begin{aligned} \dot{\mathcal{H}}(\mathbf{x}, \bar{\mathbf{x}}) &= \langle \nabla_{\mathbf{x}} \mathcal{H}(\mathbf{x}, \bar{\mathbf{x}}), \dot{\mathbf{x}} \rangle = \langle \nabla_{\mathbf{x}} \mathcal{H}(\mathbf{x}, \bar{\mathbf{x}}), \dot{\mathbf{x}} - \dot{\bar{\mathbf{x}}} \rangle \quad (8) \\ &= \langle \nabla H(\mathbf{x}) - \nabla H(\bar{\mathbf{x}}), \mathbf{F}[\nabla H(\mathbf{x}) - \nabla H(\bar{\mathbf{x}})] + \mathbf{G}(\mathbf{u} - \bar{\mathbf{u}}) \rangle \\ &= \langle \nabla H(\mathbf{x}) - \nabla H(\bar{\mathbf{x}}), \mathbf{F}[\nabla H(\mathbf{x}) - \nabla H(\bar{\mathbf{x}})] \rangle \\ &\quad + \langle \mathbf{y} - \bar{\mathbf{y}}, \mathbf{u} - \bar{\mathbf{u}} \rangle, \quad (9) \end{aligned}$$

where we subtracted $\dot{\bar{\mathbf{x}}} = 0_n$ in (8) and applied the adjoint of \mathbf{G} in (9). From (9), the shifted passivity of (4) holds as soon as $\text{He}\{\mathbf{F}\} \prec 0$. Note that if the Hamiltonian $H(\mathbf{x})$ is quadratic, then due to (7), (8), the energy balance equation (9) still holds if $\bar{\mathbf{x}}$ is not an equilibrium point, i.e., $\dot{\bar{\mathbf{x}}} \neq 0_n$. This fact is exploited to extend shifted passivity to limit cycles later. Lastly, for memoryless mappings, we have the following definition.

Definition 4 The input-output mapping $\Upsilon : \mathbb{C}^m \rightarrow \mathbb{C}^m$ is said to be shifted passive w.r.t. the steady-state input $\bar{\mathbf{u}}$ if for all \mathbf{u} , it holds that

$$0 \leq \langle \Upsilon(\mathbf{u}) - \Upsilon(\bar{\mathbf{u}}), \mathbf{u} - \bar{\mathbf{u}} \rangle. \quad (10)$$

If (10) holds for all $\bar{\mathbf{u}} \in \mathbb{C}^n$, this property is also known as equilibrium independent passivity [33], and as monotonicity [30].

3 Model of the microgrid system with DER control

In this section, we model the microgrid using the hierarchical port-Hamiltonian approach in [7]. The system is viewed as a directed graph, where the edges include the DER generator (G), R - L line (T), and shunt capacitor (C) edges, assuming the Π -model of the distribution lines [43]. Different from [7], we treat the loads, assumed static [35], as additive disturbances to the shunt capacitor dynamics. The nodes include the DER generator, standalone load, and ground node. To simplify the model, we assume i) the ground node has zero potential; ii) the R - L lines have no interior junctions. Let the microgrid comprise g DER generators, τ R - L lines, and $g + \ell$ shunt capacitors with loads that are connected from every node to the ground. The total number of edges is $n = 2g + \ell + \tau$, with the indices $e = 1, \dots, n$.³ The edges are ordered as follows. Edges 1 to g are DER generators. Edges $g + 1$ to $g + \tau$ are R - L lines. The remaining $g + \ell$ edges are shunt capacitors with loads. The edge voltage and current directions follow the direction of the edge such that the ground is always the head. The incidence matrix for the graph of the power network is given by

$$\mathbf{M} = \begin{bmatrix} \begin{bmatrix} \mathbf{I}_g \\ \mathbf{0}_{\ell \times g} \end{bmatrix} & \mathbf{M}_1 & \mathbf{I}_{g+\ell} \\ -\mathbf{1}_g^T & \mathbf{0}_\tau^T & -\mathbf{1}_{g+\ell}^T \end{bmatrix}$$

where \mathbf{M}_1 is the incidence matrix of the sub-graph obtained by removing the ground node [7].

3.1 Interconnection constraints

We assume that the microgrid is balanced, i.e., the sum of every three-phase voltage or current is zero. Then, applying the power-preserving Clarke ($\alpha\beta 0$ or stationary $dq0$) transformation [23] to every three-phase voltage or current $\mathbf{x}_{abc} = [x_a, x_b, x_c]^T$, the 0-component evaluates to zero, and the $\alpha\beta$ -components are represented by a single complex variable $x_{\alpha\beta} = x_\alpha + jx_\beta$. The mapping $\mathbf{x}_{abc} \mapsto x_{\alpha\beta}$ is linear, unitary, and both \mathbf{x}_{abc} and $x_{\alpha\beta}$ have two degrees of freedom.

As introduced later, the dynamics of each edge has the pH form (4), which are interconnected by the constraints on the port variables $(\mathbf{u}_{e,1}, \mathbf{y}_{e,1})$. Let us denote by $\underline{V} = [\underline{V}_G^T, \underline{V}_T^T, \underline{V}_C^T]^T$ the edge voltages, $\underline{I} = [\underline{I}_G^T, \underline{I}_T^T, \underline{I}_C^T]^T$ the edge currents, and $\underline{V} = [\underline{V}_C^T, 0]^T$ the node potentials. The physical constraints are given by

$$\begin{aligned} \mathbf{M}\underline{I} &= \mathbf{0}_n \text{ (KCL)}, \\ \mathbf{M}^T \underline{V} &= \underline{U} \text{ (KVL)}. \end{aligned}$$

³ To avoid confusion with other subscripts, the subscript e is never replaced by its value.

For DER generators and R - L lines, we assign the edge current as the input $\mathbf{u}_{e,1}$. For shunt capacitors, we assign the edge voltage as the input $\mathbf{u}_{e,1}$.⁴ The edge inputs and outputs are stacked into

$$\begin{aligned}\text{col}(\mathbf{u}_{e,1}) &= [\underline{V}_G^\top, \underline{V}_T^\top, \underline{I}_C^\top]^\top \\ \text{col}(\mathbf{y}_{e,1}) &= [\underline{I}_G^\top, \underline{I}_T^\top, \underline{V}_C^\top]^\top.\end{aligned}$$

We then obtain, from KCL and KVL, the interconnection constraints $\text{col}(\mathbf{u}_{e,1}) = \mathbf{W}\text{col}(\mathbf{y}_{e,1})$ where

$$\mathbf{W} = \begin{bmatrix} \mathbf{0}_{g \times g} & \mathbf{0}_{g \times T} & [\mathbf{I}_g \ \mathbf{0}_{g \times \ell}]^\top \\ \mathbf{0}_{T \times g} & \mathbf{0}_{T \times T} & \mathbf{M}_1^\top \\ \begin{bmatrix} -\mathbf{I}_g \\ \mathbf{0}_{\ell \times g} \end{bmatrix} & -\mathbf{M}_1 & \mathbf{0}_{g+\ell} \end{bmatrix}. \quad (11)$$

3.2 Edges for R - L lines ($e = g + 1, \dots, g + T$)

The equation for the R - L line is given by

$$(L_e \dot{I}_e) = -R_e I_e + V_e, \quad (12)$$

where R_e and L_e are the resistance and inductance of the R - L line. The subsystem (12) is rewritten in the pH form (4) by defining the state $\mathbf{x}_e = L_e I_e$, the input $\mathbf{u}_{e,1} = V_e$, the Hamiltonian $H_e(\mathbf{x}_e) = \frac{1}{2} L_e^{-1} \|\mathbf{x}_e\|^2$ with $\nabla H_e(\mathbf{x}_e) = I_e$, $\mathbf{F}_e = -R_e \mathbf{I}_1$, and $\mathbf{G}_{e,1} = \mathbf{I}_1$. We can find the output $\mathbf{y}_{e,1} = \mathbf{G}_{e,1}^* \nabla H_e(\mathbf{x}_e) = I_e$.

3.3 Edges for shunt capacitors with static loads ($e = g + T + 1, \dots, 2g + \ell + T$)

The equation for the shunt capacitor with the load disturbance is given by [43]

$$(C_e \dot{V}_e) = -G_e V_e + I_e - \Upsilon_e(V_e), \quad (13)$$

where C_e and G_e are the capacitance and conductance of the shunt capacitor, $\Upsilon_e(V_e)$ is the load current as a function of the bus voltage. The subsystem (13) is rewritten in the pH form (4) by defining the state $\mathbf{x}_e = C_e V_e$, the inputs $\mathbf{u}_{e,1} = I_e$, $\mathbf{u}_{e,2} = -\Upsilon_e(V_e)$, the Hamiltonian $H_e(\mathbf{x}_e) = \frac{1}{2} C_e^{-1} \|\mathbf{x}_e\|^2$ with $\nabla H_e(\mathbf{x}_e) = V_e$, $\mathbf{F}_e(\mathbf{x}_e) = -G_e \mathbf{I}_1$, and $\mathbf{G}_{e,1} = \mathbf{G}_{e,2} = \mathbf{I}_1$. The outputs are $\mathbf{y}_{e,1} = \mathbf{y}_{e,2} = V_e$.

Assumption 5 Assume that the load current function is angle-invariant, i.e., $e^{j\tau} \Upsilon_e(V_e) = \Upsilon_e(e^{j\tau} V_e)$.

⁴ Complementary inputs and outputs are chosen for interacting edges for the interconnection constraints to be a linear mapping with no additional algebraic constraints.

3.4 Edges for DER generators ($e = 1, \dots, g$)

In this subsection,⁵ equations for the closed-loop DER subsystem with the proposed controller are given. For more background, the reader is referred to [26] for the PI control in the internal reference frame and [24, 38] for the PR control in a stationary reference frame. All variables in this subsection are defined in the stationary reference frame.

I. Swing equation with approximate active power:

$$\begin{aligned}J\dot{\omega} &= -D(\omega - \omega_{\text{nom}}) - (V_{\text{nom}} \Re\{I_t e^{-j\theta}\} - P_{\text{nom}})/\omega_{\text{nom}} \\ \dot{\theta} &= \omega,\end{aligned}$$

where J is the inertia, D is the damping constant, ω_{nom} and P_{nom} are the nominal frequency and output active power, and $V_{\text{nom}} \Re\{I_t e^{-j\theta}\}$ is the approximate output active power such that the nominal voltage is used to calculate the active power instead of the instantaneous voltage. The precise active power $\Re\{I_t^* V_o\}$ is equal to the approximated active power if $V_o = V_{\text{nom}} e^{j\theta} - jX I_t$, which is achieved when the voltage controller below reaches steady state. In complex coordinates (14) is expressed as

$$\begin{aligned}J(j\omega e^{j\theta}) &= -J\omega^2 e^{j\theta} - D(j\omega e^{j\theta} - j\omega_{\text{nom}} e^{j\theta}) \\ &\quad - j e^{j\theta} (V_{\text{nom}} \Re\{I_t e^{-j\theta}\} - P_{\text{nom}})/\omega_{\text{nom}}\end{aligned} \quad (14a)$$

$$(e^{j\theta}) = j\omega e^{j\theta}. \quad (14b)$$

II. The proposed voltage controller:

$$\dot{\beta} = V_{\text{nom}} e^{j\theta} - jX I_t - V_o \quad (15a)$$

$$\dot{\xi} = j\omega_{\text{nom}} \xi + K_{iv} \beta \quad (15b)$$

$$m = \mathbf{K} [I_b, V_o, I_t, \beta, \xi]^\top, \quad (15c)$$

where β and ξ are the state variables. The parameters include the virtual reactance X [41], the gain K_{iv} , and $\mathbf{K} \in \mathbb{C}^{1 \times 5}$. The output signal m is the modulation index for the inverter to create the terminal voltage $V_t = \frac{V_{dc}}{2} m$ (ignoring the switching frequency). Intuitively, the first integrator (15a) achieves $\bar{V}_o(\tau) \approx V_{\text{nom}} e^{j\bar{\theta}(\tau)} - jX \bar{I}_t(\tau)$, and the second integrator (15b) achieves $\bar{\beta}(\tau) \approx 0$. By substituting (15a) and (15b) into the limit cycle condition, $\dot{\bar{\mathbf{x}}}(\tau) = j\bar{\omega} \bar{\mathbf{x}}(\tau)$, we obtain the steady-state voltage as:

$$\bar{V}_o(\tau) = V_{\text{nom}} e^{j\bar{\theta}(\tau)} - jX \bar{I}_t(\tau) + \frac{\bar{\omega}(\bar{\omega} - \omega_{\text{nom}})}{K_{iv}} \bar{\xi}(\tau). \quad (16)$$

⁵ The subscript e is dropped in this subsection to ease notation.

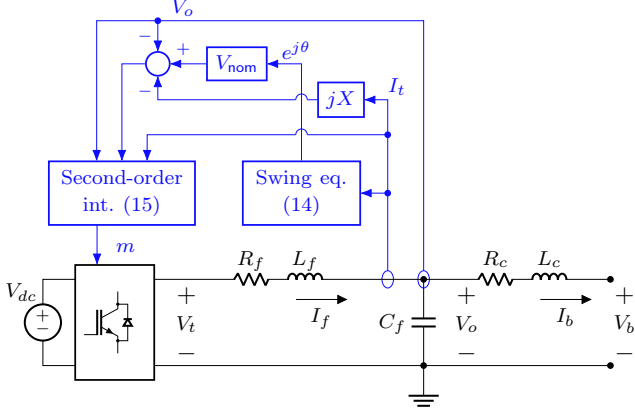


Fig. 1. Single-phase diagram of DER control system in a stationary reference frame

III. The RLC filter and the line coupling:

$$L_c \dot{I}_b = -R_c I_b + V_o - V_b \quad (17a)$$

$$C_f \dot{V}_o = I_t - I_b \quad (17b)$$

$$L_f \dot{I}_t = -R_f I_t + \frac{1}{2} V_{dc} m - V_o, \quad (17c)$$

where $V_t = \frac{1}{2} V_{dc} m$ is the inverter terminal voltage. The input and output of the DER subsystem that can interact with the network are $\mathbf{u}_1 = V_b$ and $\mathbf{y}_1 = -I_b$.

3.5 Angle symmetry of the microgrid system

Lemma 6 Consider the microgrid system consisting of the interconnection constraints (11) and the edge dynamics (12), (13), (14), (15), (17). Let Assumption 5 hold. Then this system has the symmetry $\mathcal{T}(\tau)\mathbf{x} = e^{j\tau}\mathbf{x}$.

PROOF. By Definition 2, it is equivalent to prove that the solution set of the microgrid system is invariant to $\mathcal{T}(\tau)$. We can construct the solution set Ω of the microgrid through the following two steps: i) Collect the solution sets of every edge,

$$\Omega_e \ni (\mathbf{x}_e(t), \mathbf{y}_e(t), \mathbf{u}_e(t)),$$

where the unconstrained edge inputs include all continuous functions. It is straightforward to check that every edge equation satisfies $\mathbf{f}_e(e^{j\tau}\mathbf{x}_e, e^{j\tau}\mathbf{u}_e) = e^{j\tau}\mathbf{f}_e(\mathbf{x}_e, \mathbf{u}_e)$. The outputs being linear in \mathbf{x}_e are shifted by $e^{j\tau}$ as well. ii) Keep the unconstrained edge solutions that satisfy the network and the load constraints, i.e.,

$$\Omega = \{\text{col}(\mathbf{x}_e(t)) \mid \text{col}(\mathbf{u}_e(t)) = \mathbf{W} \text{col}(\mathbf{y}_e(t)), \mathbf{u}_e(t) = \Upsilon_e(\mathbf{y}_e(t)), e = g + \mathbb{T} + 1, \dots, 2g + \ell + \mathbb{T}\}.$$

Since the interconnection constraints and the load constraints are invariant to the angle symmetry, the overall solution set Ω is invariant to the angle symmetry. \square

4 Port-Hamiltonian model of the DER subsystem

Assumption 7 Assume that the microgrid system has a circular limit cycle $\bar{\mathbf{x}}(\tau, t) = e^{j\bar{\omega}(\tau-t_0)}\bar{\mathbf{x}}(\tau, t_0)$.

In the stability proof, we first consider a modified solution set of the microgrid system where every solution is multiplied by $e^{-\kappa(t-t_0)}$ for $0 < \kappa \ll 1$. The purpose is to include a tiny amount of quadratic dissipation in the complex DER angles (14b). The equations of the microgrid system are changed from $\dot{\mathbf{x}} = \mathbf{f}(\mathbf{x}, \mathbf{u}_2)$ to $\dot{\mathbf{x}} = -\kappa\mathbf{x} + \mathbf{f}(\mathbf{x}, \mathbf{u}_2')$, where $\mathbf{u}_2'(\mathbf{x}) = e^{-\kappa(t-t_0)}\mathbf{u}_2(e^{\kappa(t-t_0)}\mathbf{x})$.

We decouple the voltage controller (15) from the swing equation (14) by incorporating an additional state variable φ into (15):⁶

$$\dot{\beta} = -\kappa\beta - \kappa\varphi - jXI_t - V_o \quad (18a)$$

$$\dot{\varphi} = j\omega\varphi - \kappa\varphi \quad (18b)$$

$$\dot{\xi} = -\kappa\xi + j\omega_{\text{nom}}\xi + K_{iv}\beta \quad (18c)$$

$$m = \mathbf{K} [I_b, V_o, I_t, \beta, \xi]^T. \quad (18d)$$

Let us fix $\varphi(t_0) = \bar{\varphi}(\tau, t_0) = -V_{\text{nom}}/\kappa$. Then, the magnitude $|\varphi| = |\bar{\varphi}(\tau)|$ is determined for all time from (18b), and we have

$$-\kappa\varphi = e^{-\kappa(t-t_0)}V_{\text{nom}}e^{j\theta}, \quad (19)$$

which is the shrinking internal reference voltage; similarly for the steady-state solution.

To express the DER subsystem in pH form, we replace β and φ by $\beta_1 = \beta + \varphi$ and $\beta_2 = \beta - \varphi$ to transform (18) into

$$\begin{aligned} \dot{\beta}_1 &= j\frac{\omega}{2}(\beta_1 - \beta_2) - jXI_t - V_o - \frac{3}{2}\kappa\beta_1 + \frac{1}{2}\kappa\beta_2 \\ \dot{\beta}_2 &= -j\frac{\omega}{2}(\beta_1 - \beta_2) - jXI_t - V_o - \frac{1}{2}\kappa\beta_1 - \frac{1}{2}\kappa\beta_2 \\ \dot{\xi} &= -\kappa\xi + j\omega_{\text{nom}}\xi + K_{iv}\frac{\beta_1 + \beta_2}{2} \\ m &= \mathbf{K} [I_b, V_o, I_t, \frac{\beta_1 + \beta_2}{2}, \xi]^T. \end{aligned} \quad (20)$$

Eq. (17) is transformed into

$$\begin{aligned} L_c \dot{I}_b &= -\kappa L_c I_b - R_c I_b + V_o - V_b \\ C_f \dot{V}_o &= -\kappa C_f V_o + I_t - I_b \\ L_f \dot{I}_t &= -\kappa L_f I_t - R_f I_t + \frac{1}{2} V_{dc} m - V_o. \end{aligned} \quad (21)$$

⁶ For simplicity, we refrain from creating a different notation for the shrinking states. The latter are assumed until Proposition 12, where we remove the effect of shrinking in (41).

Define the state vector

$$\mathbf{x} = [x_1, \dots, x_6]^\top = [L_c I_b, C_f V_o, L_f I_t, \beta_1, \beta_2, \xi]^\top.$$

Define the Hamiltonian function as $H(\mathbf{x}) = \frac{1}{2} \|\mathbf{x}\|_{\hat{\mathbf{Q}}}^2$ with

$$\mathbf{Q} = \text{diag}(L_c^{-1}, C_f^{-1}, L_f^{-1}, 1, 1, 1).$$

The gradient is

$$\nabla H(\mathbf{x}) = \mathbf{Q}\mathbf{x} = [I_b, V_o, I_t, \beta_1, \beta_2, \xi]^\top. \quad (22)$$

Define the input and output as $\mathbf{u}_1 = V_b$ and $\mathbf{y}_1 = -I_b$. We can then compile (21) and (20) into the pH system:

$$\dot{\mathbf{x}} = \mathbf{F}\nabla H(\mathbf{x}) + j\frac{\omega}{2}\mathbf{F}_3\mathbf{x} + \mathbf{G}\mathbf{u}_1 \quad (23a)$$

$$\mathbf{y}_1 = \mathbf{G}^*\nabla H(\mathbf{x}), \quad (23b)$$

where

$$\begin{aligned} \mathbf{F} &= \mathbf{F}_1 - \kappa\mathbf{F}_2, \mathbf{F}_1 = \mathbf{F}_0 + \mathbf{B}\mathbf{K}_1, \\ \mathbf{F}_0 &= \begin{bmatrix} -R_c & 1 & 0 & 0 & 0 & 0 \\ -1 & 0 & 1 & 0 & 0 & 0 \\ 0 & -1 & -R_f & 0 & 0 & 0 \\ 0 & -1 & -jX & 0 & 0 & 0 \\ 0 & -1 & -jX & 0 & 0 & 0 \\ 0 & 0 & 0 & \frac{K_{iv}}{2} & \frac{K_{iv}}{2} & j\omega_{\text{nom}} \end{bmatrix}, \\ \mathbf{F}_2 &= \text{diag}(1, 1, 1, [\frac{3}{2}, -\frac{1}{2}, \frac{1}{2}, \frac{1}{2}], 1), \\ \mathbf{F}_3 &= \text{diag}(0, 0, 0, [1, -1; -1, 1], 0), \\ \mathbf{G} &= -\mathbf{e}_1, \mathbf{B} = \frac{V_{dc}}{2}\mathbf{e}_3. \end{aligned} \quad (24)$$

Remark 8 The gain \mathbf{K}_1 in (24) is equivalent to the gain \mathbf{K} in (21): The 4-th and 5-th columns of \mathbf{K}_1 are equal to $\frac{1}{2}$ times the 4-th column of \mathbf{K} . The remaining columns of \mathbf{K}_1 are equal to those of \mathbf{K} at appropriate positions.

5 Energy balance equations

The goal is to derive the energy balance for the shifted Hamiltonian defined with respect to the limit cycle $\bar{\mathbf{x}}(\tau)$ that shrinks exponentially at the rate of κ . The phase τ is initially assumed to be a constant.

5.1 Energy balance for each edge

Edges for DER generators. Analogous to the Lyapunov method in linear control,⁷ we will derive the energy balance for the candidate storage function $\hat{H}(\mathbf{x}) = \frac{1}{2} \|\mathbf{x}\|_{\hat{\mathbf{Q}}}^2$

⁷ The subscript e is dropped for the DER subsystem.

where $\hat{\mathbf{Q}} = \mathbf{P}\mathbf{Q} = \mathbf{Q}\mathbf{P}^* \succ 0$ and

$$\mathbf{P} = \text{diag}(1, \mathbf{P}_{22}) \quad (25)$$

for $\mathbf{P}_{22} \in \mathbb{C}^{5 \times 5}$. The chosen structure of \mathbf{P} in (25) preserves the output: $-I_b e^{j\theta} = \mathbf{G}^* \nabla H(\mathbf{x}) = \mathbf{G}^* \nabla \hat{H}(\mathbf{x})$. Define the co-energy states $\mathbf{s} = \mathbf{Q}\mathbf{x}$ and $\bar{\mathbf{s}}(\tau) = \mathbf{Q}\bar{\mathbf{x}}(\tau)$. We make the following assumption to reduce the space of candidate storage functions to search.

Assumption 9 Assume that the 4-th row of $\hat{\mathbf{Q}} = \mathbf{P}\mathbf{Q}$ is equal to the 5-th row except for the 2-by-2 diagonal block, which is equal to $q_4 \mathbf{I}_2$ for $q_4 > 0$.

Based on (8), the energy balance equation for the candidate storage function writes

$$\begin{aligned} \dot{\hat{H}}(\mathbf{x}, \bar{\mathbf{x}}(\tau)) &= \langle \nabla \hat{H}(\mathbf{x}) - \nabla \hat{H}(\bar{\mathbf{x}}(\tau)), \dot{\mathbf{x}} - \dot{\bar{\mathbf{x}}}(\tau) \rangle \\ &= \langle \nabla \hat{H}(\mathbf{x}) - \nabla \hat{H}(\bar{\mathbf{x}}(\tau)), \mathbf{F}[\nabla H(\mathbf{x}) - \nabla H(\bar{\mathbf{x}}(\tau))] \rangle \\ &\quad + \langle \nabla \hat{H}(\mathbf{x}) - \nabla \hat{H}(\bar{\mathbf{x}}(\tau)), \mathbf{F}_3[j\frac{\omega}{2}\mathbf{x} - j\frac{\omega}{2}\bar{\mathbf{x}}(\tau)] \rangle \\ &\quad + \langle \nabla \hat{H}(\mathbf{x}) - \nabla \hat{H}(\bar{\mathbf{x}}(\tau)), \mathbf{G}[\mathbf{u} - \bar{\mathbf{u}}(\tau)] \rangle \\ &= \langle \mathbf{s} - \bar{\mathbf{s}}(\tau), \mathbf{P}^*\mathbf{F}[\mathbf{s} - \bar{\mathbf{s}}(\tau)] \rangle \\ &\quad + \langle \mathbf{x} - \bar{\mathbf{x}}(\tau), \mathbf{Q}\mathbf{P}^*\mathbf{F}_3[j\frac{\omega}{2}\mathbf{x} - j\frac{\omega}{2}\bar{\mathbf{x}}(\tau)] \rangle \\ &\quad + \langle \mathbf{y}_1 - \bar{\mathbf{y}}_1(\tau), \mathbf{u}_1 - \bar{\mathbf{u}}_1(\tau) \rangle. \end{aligned} \quad (26)$$

The 2-nd term in the RHS of (26) can be derived as

$$\begin{aligned} \langle \mathbf{x} - \bar{\mathbf{x}}(\tau), \mathbf{Q}\mathbf{P}^*\mathbf{F}_3[j\frac{\omega}{2}\mathbf{x} - j\frac{\omega}{2}\bar{\mathbf{x}}(\tau)] \rangle \\ = \langle \mathbf{x} - \bar{\mathbf{x}}(\tau), q_4 \mathbf{F}_3[j\frac{\omega}{2}\mathbf{x} - j\frac{\omega}{2}\bar{\mathbf{x}}(\tau)] \rangle \\ = 2q_4 \langle \varphi - \bar{\varphi}(\tau), j\omega\varphi - j\omega\bar{\varphi}(\tau) \rangle. \end{aligned} \quad (27)$$

Based on (26), (27), and the definition (29), the energy balance equation for $\hat{H}(\mathbf{x}, \bar{\mathbf{x}}(\tau))$ is obtained as

$$\begin{aligned} \dot{\hat{H}}(\mathbf{x}, \bar{\mathbf{x}}(\tau)) &= \|\mathbf{s} - \bar{\mathbf{s}}(\tau)\|_{\text{He}\{\mathbf{P}^*\mathbf{F}\}}^2 \\ &\quad + 2q_4 \langle \varphi - \bar{\varphi}(\tau), j\omega\varphi - j\omega\bar{\varphi}(\tau) \rangle \\ &\quad + \langle \mathbf{y}_1 - \bar{\mathbf{y}}_1(\tau), \mathbf{u}_1 - \bar{\mathbf{u}}_1(\tau) \rangle. \end{aligned} \quad (28)$$

It will be shown that the first term in (28) can be made negative definite with an appropriate choice of \mathbf{K}_1 . For the second term in (28), we will define a function $\hat{\tau}$ of the state of the overall microgrid and substituting $\tau = \hat{\tau}$ such that the second term in (28) cancels with $\frac{\partial}{\partial \tau} \hat{H}(\mathbf{x}, \bar{\mathbf{x}}(\hat{\tau})) \frac{d}{dt} \hat{\tau}$. The function $\hat{\tau}$ is defined later in Subsection 5.2. Here, we can gain more insight into the shifted Hamiltonian by noting the following decomposition:

$$\hat{H}(\mathbf{x}, \bar{\mathbf{x}}(\tau)) = \tilde{H}(\mathbf{x}, \bar{\mathbf{x}}(\tau)) + q_4 \|\varphi - \bar{\varphi}(\tau)\|^2, \quad (29)$$

where we have $\tilde{H}(\mathbf{x}, \bar{\mathbf{x}}(\tau)) = \frac{1}{2} \|\mathbf{x} - \bar{\mathbf{x}}(\tau)\|_{\tilde{\mathbf{Q}}}^2$, and $\tilde{\mathbf{Q}}$ is modified from $\hat{\mathbf{Q}}$ by replacing the diagonal block $q_4 \mathbf{I}_2$

with $q_4 [\frac{1}{2}, \frac{1}{2}; \frac{1}{2}, \frac{1}{2}]$. Equivalently,

$$\tilde{\mathbf{Q}} = \mathbf{N}\mathbf{N}^\dagger \hat{\mathbf{Q}} \mathbf{N}\mathbf{N}^\dagger$$

where

$$\mathbf{N} = \text{diag}(1, 1, 1, [1; 1], 1).$$

Hence, $\tilde{\mathbf{Q}} \succeq 0$ and $\tilde{\mathcal{H}}(\mathbf{x}, \bar{\mathbf{x}}(\tau)) \geq 0$. Clearly, $\tilde{\mathcal{H}}(\mathbf{x}, \bar{\mathbf{x}}(\tau))$ is dependent on $\frac{1}{2}(\beta_1 + \beta_2) = \beta$ and is independent of $\frac{1}{2}(\beta_1 - \beta_2) = \varphi$.

Edges for R - L lines. By (12) and (9), the energy balance for every R - L line edge is

$$\begin{aligned} \dot{\mathcal{H}}_e(\mathbf{x}_e, \bar{\mathbf{x}}_e(\tau)) = & -(\kappa L_e + R_e) \|I_e - \bar{I}_e(\tau)\|^2 \\ & + \langle \mathbf{y}_{e,1} - \bar{\mathbf{y}}_{e,1}(\tau), \mathbf{u}_{e,1} - \bar{\mathbf{u}}_{e,1}(\tau) \rangle. \end{aligned} \quad (30)$$

Edges for shunt capacitors. By (13) and (9), the energy balance for every shunt capacitor edge is

$$\begin{aligned} \dot{\mathcal{H}}_e(\mathbf{x}_e, \bar{\mathbf{x}}_e(\tau)) = & -(\kappa C_e + G_e) \|V_e - \bar{V}_e(\tau)\|^2 \\ & + \langle V_e - \bar{V}_e(\tau), \Upsilon'_e(t, V_e) - \Upsilon'_e(t, \bar{V}_e(\tau)) \rangle \\ & + \langle \mathbf{y}_{e,1} - \bar{\mathbf{y}}_{e,1}(\tau), \mathbf{u}_{e,1} - \bar{\mathbf{u}}_{e,1}(\tau) \rangle, \end{aligned} \quad (31)$$

where $\Upsilon'_e(t, V) = e^{-\kappa(t-t_0)} \Upsilon_e(e^{\kappa(t-t_0)} V)$. For simplicity, we assume that all loads are globally shifted passive. On the other hand, if not all loads are globally passive [34], it is relatively straightforward to estimate the region of attraction by considering the shifted passivity boundaries of the loads.

Assumption 10 Assume that the load $\Upsilon_e(V_e)$ is globally shifted passivity with respect to all $\bar{V}_e \in \mathbb{C}$.

Then, it implies

$$\begin{aligned} & \langle V_e - \bar{V}_e(\tau), \Upsilon'_e(t, V_e) - \Upsilon'_e(t, \bar{V}_e(\tau)) \rangle \\ & = \langle e^{-\kappa(t-t_0)} V_e - e^{-\kappa(t-t_0)} \bar{V}_e(\tau), \dots \\ & \quad \Upsilon_e(e^{-\kappa(t-t_0)} V_e) - \Upsilon_e(e^{-\kappa(t-t_0)} \bar{V}_e(\tau)) \rangle \leq 0. \end{aligned}$$

5.2 Overall energy balance

Define the shifted Hamiltonian of the overall microgrid as $\mathcal{H} = \sum_{e=1}^g \hat{\mathcal{H}}_e + \sum_{e=g+1}^n \mathcal{H}_e$. Summing the energy balance equations for every edge, the input shifted power cancels as a consequence of the skew-symmetric interconnection constraints in (11), i.e.,

$$\begin{aligned} & \langle \text{col}(\mathbf{y}_{e,1} - \bar{\mathbf{y}}_{e,1}(\tau)), \text{col}(\mathbf{u}_{e,1} - \bar{\mathbf{u}}_{e,1}(\tau)) \rangle \\ & = \langle \text{col}(\mathbf{y}_{e,1} - \bar{\mathbf{y}}_{e,1}(\tau)), \mathbf{W}[\text{col}(\mathbf{y}_{e,1} - \bar{\mathbf{y}}_{e,1}(\tau))] \rangle = 0. \end{aligned}$$

We then obtain the overall energy balance as

$$\begin{aligned} \dot{\mathcal{H}}(\mathbf{x}, \bar{\mathbf{x}}(\tau)) \leq & \sum_{e=1}^g \|\mathbf{s}_e - \bar{\mathbf{s}}_e(\tau)\|_{\text{He}\{\mathbf{P}_e^* \mathbf{F}_e\}}^2 \\ & + \sum_{e=1}^g 2q_{e,4} \langle \varphi_e - \bar{\varphi}_e(\tau), j\omega_e \varphi_e - j\bar{\omega}_e \bar{\varphi}_e(\tau) \rangle \\ & - \sum_{e=g+1}^{g+T} (\kappa L_e + R_e) \|I_e - \bar{I}_e(\tau)\|^2 \\ & - \sum_{e=g+T+1}^n (\kappa C_e + G_e) \|V_e - \bar{V}_e(\tau)\|^2. \end{aligned} \quad (32)$$

As mentioned above, let us define $\hat{\tau}$ as a solution of the following time-varying differential equation:

$$\begin{aligned} 0 = & \frac{\partial}{\partial \tau} \mathcal{H}(\mathbf{x}, \bar{\mathbf{x}}(\tau)) \dot{\tau} \dots \\ & + \sum_{e=1}^g 2q_{e,4} \langle \varphi_e - \bar{\varphi}_e(\tau), j\omega_e \varphi_e - j\bar{\omega}_e \bar{\varphi}_e(\tau) \rangle, \end{aligned} \quad (33)$$

which can be expressed as

$$\begin{aligned} 0 = & \left[\sum_{e=1}^g \langle \mathbf{x}_e, j\tilde{\mathbf{Q}}_e \bar{\mathbf{x}}_e(\tau) \rangle + \sum_{e=g+1}^{g+T} \langle I_e, jL_e \bar{I}_e(\tau) \rangle \dots \right. \\ & \left. + \sum_{e=g+T+1}^n \langle V_e, jG_e \bar{V}_e(\tau) \rangle \right] \dot{\tau} + \frac{d}{dt} \sum_{e=1}^g q_{e,4} \|\varphi_e - \bar{\varphi}_e(\tau)\|^2, \end{aligned} \quad (34)$$

where the last derivative is with respect to the original system (without the shrinking effect). Note that (33) is solvable in the set $E = \{\mathbf{x} \mid \frac{\partial}{\partial \tau} \mathcal{H}(\mathbf{x}, \bar{\mathbf{x}}(\tau)) \neq 0\}$, which is almost everywhere in \mathbb{C}^n ($n = 8g + 2\ell + 2T$). Then, we make the following simplifying assumption.

Assumption 11 Assume every solution of the microgrid system belongs to the set E for almost all $t \in \mathbb{R}$.

Assumption 11 is justified by noting that the Hamiltonian can be slightly perturbed independently of the behavior of the system to obtain a different set E .

Substituting (33) into (32), we obtain

$$\begin{aligned} \dot{\mathcal{H}}(\mathbf{x}, \bar{\mathbf{x}}(\hat{\tau})) \leq & \sum_{e=1}^g \|\mathbf{s}_e - \bar{\mathbf{s}}_e(\hat{\tau})\|_{\text{He}\{\mathbf{P}_e^* \mathbf{F}_e\}}^2 \\ & - \sum_{e=g+1}^{g+T} (\kappa L_e + R_e) \|I_e - \bar{I}_e(\hat{\tau})\|^2 \\ & - \sum_{e=g+T+1}^n (\kappa C_e + G_e) \|V_e - \bar{V}_e(\hat{\tau})\|^2. \end{aligned} \quad (35)$$

5.3 Main result

The main stability result is stated as follows. Define the notation $\tilde{\mathbf{F}}_{e,1} = \mathbf{N}^\dagger \mathbf{F}_{e,1} \mathbf{N}$ and $\tilde{\mathbf{P}}_e = \mathbf{N}^* \mathbf{P}_e \mathbf{N}$.

Proposition 12 *Assume that $\text{He}\{\tilde{\mathbf{P}}_e^* \tilde{\mathbf{F}}_{e,1}\} \prec 0$ for $e = 1, \dots, g$. Assume that the circular limit cycle $\bar{\mathbf{x}}(\tau)$ from Assumption 7 is the only circular limit cycle of the system. Then, the orbit of $\bar{\mathbf{x}}(\tau)$ is globally attractive.*

PROOF. From (35), we have that $\dot{\mathcal{H}}(\mathbf{x}, \bar{\mathbf{x}}(\hat{\tau})) \leq 0$ if, for $e = 1, \dots, g$, it holds that

$$\text{He}\{\mathbf{P}_e^* \mathbf{F}_e\} \prec 0, \quad (36)$$

which can be expanded into

$$\text{He}\{\mathbf{P}_e^* \mathbf{F}_{e,1}\} - \kappa \text{He}\{\mathbf{P}_e^* \mathbf{F}_{e,2}\} \prec 0 \quad (37)$$

Note that the row and column spaces of the matrix $\text{He}\{\mathbf{P}_e^* \mathbf{F}_{e,1}\}$ are equal to the column space of \mathbf{N} . By the assumption, there exists an $a > 0$ such that

$$\text{He}\{\tilde{\mathbf{P}}_e^* \tilde{\mathbf{F}}_{e,1}\} + a(\mathbf{N}^\dagger)^* \mathbf{N}^\dagger \prec 0. \quad (38)$$

Now, to prove (37), it suffices to prove that

$$-a(\mathbf{N}^\dagger)^* \mathbf{N}^\dagger - \kappa \text{He}\{\mathbf{P}_e^* \mathbf{F}_{e,2}\} \prec 0. \quad (39)$$

It is not difficult to verify, from the definition of $\mathbf{F}_{e,2}$ in (24) and Assumption 9, that all elements on the main diagonal of $\text{He}\{\tilde{\mathbf{Q}}_e \mathbf{F}_{e,2}\} = \text{He}\{\mathbf{Q}_e \mathbf{P}_e^* \mathbf{F}_{e,2}\}$ are positive, and the same holds for $\text{He}\{\mathbf{P}_e^* \mathbf{F}_{e,2}\}$. Now, consider the following decomposition:

$$2\text{He}\{\mathbf{P}_e^* \mathbf{F}_{e,2}\} = \mathbf{Q}_1 + \mathbf{Q}_2,$$

where \mathbf{Q}_1 keeps the 4-th and 5-th rows and columns of $2\text{He}\{\mathbf{P}_e^* \mathbf{F}_{e,2}\}$, and \mathbf{Q}_2 keeps the rest. Denote by \mathbf{N}_1 the identity matrix with the 4-th and 5-th diagonal element replaced by zero. We obtain the following sufficient condition for (39):

$$\begin{cases} -a\mathbf{N}_1 - \kappa\mathbf{Q}_1 \prec 0, \\ -a\mathbf{N}_1 - \kappa\mathbf{Q}_2 \preceq 0. \end{cases} \quad (40)$$

We claim that condition (40) holds for small enough κ . For the first inequality, we can take the Schur complement of the 2-by-2 diagonal block between the 4-th and 5-th row of the LHS to see that it holds for small enough κ . By construction, the second inequality holds for small enough κ . Hence, (40) holds for small enough κ , which implies (36).

Recall from Section 4 that the solutions of the system are artificially shrunk by $e^{-\kappa(t-t_0)}$. We can remove this

artificial shrinking from the energy balance equation to obtain $\dot{\mathcal{H}}(\mathbf{x}, \bar{\mathbf{x}}(\hat{\tau})) \leq 2\kappa \mathcal{H}(\mathbf{x}, \bar{\mathbf{x}}(\hat{\tau}))$, or equivalently,

$$\frac{d}{dt} \log(\mathcal{H}(\mathbf{x}, \bar{\mathbf{x}}(\hat{\tau}))) \leq 2\kappa. \quad (41)$$

Notice that, if we fix the scale of φ , from (29) and (19), we can express $\mathcal{H}(\mathbf{x}, \bar{\mathbf{x}}(\tau))$ as

$$\mathcal{H}(\mathbf{x}, \bar{\mathbf{x}}(\tau)) = \tilde{\mathcal{H}}(\mathbf{x}, \bar{\mathbf{x}}(\tau)) + \sum_{e=1}^g \kappa^{-2} q_4 \|\varphi - \bar{\varphi}(\tau)\|^2, \quad (42)$$

where $\tilde{\mathcal{H}}(\mathbf{x}, \bar{\mathbf{x}}(\tau))$ is a quadratic function not dependent on κ . Notice also that, by the definition of $\hat{\tau}$, the derivative of the second term in (42) is canceled. Hence (41) can be expressed as

$$\frac{d}{dt} \log(\tilde{\mathcal{H}}(\mathbf{x}, \bar{\mathbf{x}}(\hat{\tau}))) \leq 2\kappa, \quad (43)$$

By taking $\kappa \rightarrow 0$, $\hat{\tau}$ converges to a certain function according to (34), and we obtain that $\tilde{\mathcal{H}}(\mathbf{x}, \bar{\mathbf{x}}(\hat{\tau})) \leq 0$ in the limit. Then, applying the monotone convergence theorem, we obtain that $\mathcal{H}(\mathbf{x}, \bar{\mathbf{x}}(\hat{\tau}))$ is convergent as $t \rightarrow \infty$.

Note that $\tilde{\mathcal{H}}(\mathbf{x}, \bar{\mathbf{x}}(\tau))$ is a quadratic function in the form of $\|\mathbf{x} - \bar{\mathbf{x}}(\hat{\tau})\|_{\mathbf{Q}}^2$. From the above, the limiting solution satisfies

$$\|\mathbf{x} - \bar{\mathbf{x}}(\hat{\tau})\|_{\mathbf{Q}} = c. \quad (44)$$

for some constant c . Denote by $n = 8g + 2\ell + 2T$ the dimension of \mathbf{x} , i.e., $\mathbf{x} \in \mathbb{C}^n$. Note that the inequality (43) only depends on the linear part of the system, i.e., decoupled from φ_e , and the linear part of the system is Hurwitz from (35) and the condition in the proposition statement. Hence, without violating Assumption 9,⁸ we can perturb \mathbf{Q} to reach the same inequality (43). Let us

consider the norm $\|\mathbf{y}\|_{ij} = \sqrt{\langle \mathbf{y}, \text{He}\{\mathbf{Q} + \epsilon \hat{\mathbf{N}}_e \mathbf{e}_i^* \hat{\mathbf{N}}^*\} \mathbf{y} \rangle}$ for $0 < \epsilon \ll 1$ and $1 \leq i \leq j \leq n - g$, where $\hat{\mathbf{N}} = \text{diag}(\mathbf{I}_g \otimes \mathbf{N}, \mathbf{I}_{g+\ell+T})$. We then obtain⁹

$$\langle x_i - \bar{x}_i(\hat{\tau}), x_j - \bar{x}_j(\hat{\tau}) \rangle = c_{ij} \quad (45)$$

for some constant c_{ij} . Note that (45) entails $2n - 1$ real constraints on the limiting solution, which include

- constant $\|x_i(t) - \bar{x}_i(\hat{\tau})\|$,
- constant $\arg(x_i(t) - \bar{x}_i(\hat{\tau})) - \arg(x_i(t) - \bar{x}_j(\hat{\tau}))$.

Then, the limiting solution can only evolve in the direction of the angle symmetry, i.e., it has a circular orbit.

⁸ Assumption 9 implies that $\tilde{\mathcal{H}}(\mathbf{x}, \bar{\mathbf{x}}(\hat{\tau}))$ and $\tilde{\mathcal{H}}(\mathbf{x}, \bar{\mathbf{x}}(\hat{\tau}))$ are independent of φ_e and $\varphi_e(\hat{\tau})$.

⁹ The convergence of $\varphi_e - \bar{\varphi}_e(\hat{\tau})$ at the limiting solution can be proved by the invariance principle.

By the assumption on the uniqueness of the circular orbit of $\bar{\mathbf{x}}(\tau)$, it is the only positive limit set, which completes the proof. \square

Three comments are in order. Let us consider the scenario where κ is small. On one hand, the shifted Hamiltonian from (29) is dominated by $\sum_{e=1}^g q_{e,4} \|\varphi_e - \bar{\varphi}_e(\tau)\|^2$ since $|\varphi_e| \sim 1/\kappa$. On the other hand, the time-varying phase $\hat{\tau}$ in (34) is defined to cancel the time derivative of $\sum_{e=1}^g q_{e,4} \|\varphi_e - \bar{\varphi}_e(\tau)\|^2$ by “averaging” the DER frequencies. Here, the “average” is defined in terms of $p_{e,4}$, i.e., the diagonal elements of the Hamiltonian associated with the state variable β_e , rather than the inertia constants J_e [17]. This “averaging” essentially isolates the phase synchronization process from the energy dissipation process. The latter allows us to prove the attractivity of the periodic orbit.

To remove the effect of shrinking, the shifted passivity condition in Proposition 12 only implies that the shifted Hamiltonian is non-increasing. This is in contrast with the equilibrium point case, where the dissipation of energy is directly correlated to the quadratic dissipation matrix. The explanation is as follows: The system has angle symmetry, which means that the circular limit cycle cannot be attractive in phase. Since two limit cycles with different phases maintain a constant distance from each other, the maximal condition to impose on the energy function is for it to be non-increasing. Hence, stability is not proved in terms of the usual Lyapunov stability of the periodic orbit as a compact set [3, 44].

The proposed control ensures global attractivity of the periodic orbit, which implies frequency synchronization and voltage stability, regardless of the inertia constant J_e of the grid-forming DERs. This is a significant departure from the operational philosophy of the traditional power system, which relies on inertia to guarantee system stability. Since inertia does not affect stability with the proposed control, smaller inertia may lead to shorter settling times for power and frequency, with respect to the time constants of the distribution lines. It would be a potential future direction to study the optimal combination of J_e and D_e for more effective power sharing and smaller frequency deviation, based on the proposed control scheme that separates their choice from the stability of the system.

6 Design of the DER control gain

From Proposition 12, the stability condition writes¹⁰

$$\text{He}\{\check{\mathbf{P}}^* \check{\mathbf{F}}_1\} \prec 0, \quad (46a)$$

$$\check{\mathbf{P}}\check{\mathbf{Q}} = \check{\mathbf{Q}}^*\check{\mathbf{P}}^* \succ 0. \quad (46b)$$

¹⁰ The subscript e is omitted in this section.

where $\check{\mathbf{Q}} = \mathbf{N}^\dagger \mathbf{Q} \mathbf{N}$. Define:

$$\check{\mathbf{K}}_1 = \mathbf{K}_1 \mathbf{N} = \mathbf{K}, \quad \check{\mathbf{F}}_0 = \mathbf{N}^\dagger \mathbf{F}_0 \mathbf{N}, \quad \check{\mathbf{B}} = \mathbf{N}^\dagger \mathbf{B},$$

and $\check{\mathbf{Q}}_{22}$ as the 4-by-4 lower-right submatrix of $\check{\mathbf{Q}}$. Left and right multiplying (46a) by $(\check{\mathbf{P}}^{-1})^*$ and $\check{\mathbf{P}}^{-1}$, we obtain the equivalent condition

$$\text{He}\{\check{\mathbf{F}}_1 \check{\mathbf{P}}^{-1}\} = \text{He}\{\check{\mathbf{F}}_0 \check{\mathbf{P}}^{-1} + \check{\mathbf{B}} \mathbf{K} \check{\mathbf{P}}^{-1}\} \prec 0 \quad (47)$$

The control design problem can then be formulated [28] as the following linear matrix inequalities by choosing the unknowns as $\mathbf{L} = \mathbf{K} \mathbf{P}^{-1}$, $\mathbf{X} = \mathbf{X}^* = (\mathbf{P} \mathbf{Q})^{-1}$.

Problem 13 (Design of the DER control gain)

$$\min_{\mathbf{L} \in \mathbb{C}^{1 \times 5}, \mathbf{X}_{22} = \mathbf{X}_{22}^* \in \mathbb{C}^{4 \times 4} \succ 0} c_1 \alpha + c_2 \zeta + c_3 \gamma \quad \text{s.t.}$$

$$\begin{bmatrix} \text{He}(\check{\mathbf{F}}_0 \check{\mathbf{P}}^{-1} + \check{\mathbf{B}} \mathbf{L}) & (\check{\mathbf{P}}^{-1})^* \\ \check{\mathbf{P}}^{-1} & -\gamma \mathbf{I}_5 \end{bmatrix} \preceq 0, \quad (48)$$

$$\begin{bmatrix} \alpha \mathbf{I}_5 & \mathbf{L}^* \\ \mathbf{L} & 1 \end{bmatrix} \succeq 0, \quad \begin{bmatrix} \mathbf{Z}_{22} & \mathbf{I}_4 \\ \mathbf{I}_4 & \zeta \mathbf{I}_4 \end{bmatrix} \succeq 0, \quad (49)$$

$$\alpha, \zeta, \gamma \geq 0, \quad \check{\mathbf{P}}^{-1} = \text{diag}(1, \check{\mathbf{P}}_{22}^{-1}), \quad \check{\mathbf{P}}_{22}^{-1} = \check{\mathbf{Q}}_{22} \mathbf{X}_{22}.$$

The resulting control gain is recovered by $\mathbf{K} = \mathbf{L} \check{\mathbf{P}}$.

Regularization introduced in Problem 13 are explained as follows:

- 1) Using Schur complement, we can rewrite (48) as

$$\check{\mathbf{F}}_0 \check{\mathbf{P}}^{-1} \preceq -\gamma^{-1} (\check{\mathbf{P}}^{-1})^* \check{\mathbf{P}}^{-1},$$

which is equivalent to $\check{\mathbf{P}}^* \check{\mathbf{F}}_1 \preceq -\gamma^{-1} \mathbf{I}_5$. Hence by (32), γ^{-1} is a lower bound for the dissipation level of the DER.

- 2) The regularization in (49) can be rewritten as the following bounds,

$$\mathbf{L}^* \mathbf{L} \preceq \alpha \mathbf{I}_5, \quad \mathbf{Z}_{22} \preceq \zeta \mathbf{I}_4.$$

Remark 14 The same idea of searching for another candidate quadratic Hamiltonian in control gain design can be found in [13]. However, in [13] only three simple matrix types are considered as candidates for $\check{\mathbf{P}}$ whereas the precise condition is $\check{\mathbf{P}} \check{\mathbf{Q}} = (\check{\mathbf{P}} \check{\mathbf{Q}})^* \succ 0$.

7 Numerical example

The goal is to test the feasibility of the control gain design in Problem 13, to simulate the transient dynamics of a microgrid test system under perturbations that include load changes and disconnection/reconnection between different parts of the microgrid and the main grid,

Table 1

Parameters for the numerical example

Description	Parameter
Per-unit base	$V_{BL-L} = 400$ V, $P_B = 1$ MW, $\omega_{nom} = 60$ Hz
RLC filter	$R_f = 0.1$ Ω , $L_f = 1.35$ mH, $C_f = 50$ μ F
Line coupling	$R_c = 0.14$ Ω , $L_c = 1.6 \times 10^{-7}$ mH
Proposed reference-frame based control	
Swing equation	$D = 0.05$ pu, $J = 2$ pu
Misc.	$X = 0.4$ pu, $V_n = 1$ pu, $V_{dc} = 2$ pu,
Hyperparam.	$K_{iv} = 2 \times 10^4$, $c_1 = 1$, $c_2 = 10^2$, $c_3 = 10^5$
$\mathbf{K} = [117 - j0.5, -129, -115 - j0.3, 1293 - j4471, -49.9 - j11.6]$	
Baseline droop control (designed with $P_B = 0.1$ MW)	
Droop gains	$m_p = 0.005$ [60Hz], $n_q = 0.0667$
Input filter cutoff	$\omega_c = 6$ Hz
Double loop PI gains	$K_{pv} = 0.1833$, $K_{iv} = 230.94$, $K_{pc} = 7.59$, $K_{ic} = 4.48 \times 10^4$, $K_f = 0.75$
Microgrid test system	
ZIP load	$Z_{ld} = 65.29 + j48.97$ pu, $I_{ld} = 0$ pu, $S_{ld} = (1 + j0.75) \times 10^{-3}$ pu
Shunt capacitor	$G_{sh} = 0$ S, $C_{sh} = 16$ μ F

and to compare its transient responses with the standard droop control with the cascaded double loop PI control. The latter is designed in the frequency domain with the time scale separation assumption as specified in [26].

7.1 Verifying the feasibility of the control design

The parameters for Problem 13 in this test are provided in Table 1. All quantities are per unit except for the frequencies, which are in Hz. The RLC filter parameters are chosen as in [26] to attenuate the switching frequency of the inverter. The steady-state droop characteristic of the control is determined by D for the frequency droop and X for the voltage droop, which are respectively chosen for the microgrid system to have 0.5% nominal frequency droop at 0.1 MW active power output and 5% voltage droop at 0.075 MVA reactive power output. The inertial J is chosen so that the swing equation has a time constant of 0.1 s. The matrices in (48) are obtained from (24) with $\omega_{nom} = 60$ Hz. The parameter K_{iv} is chosen as 2×10^4 because in control gain validation, we find that larger K_{iv} results in a \mathbf{K} that provides a faster convergence rate of the system under load changes. This value for K_{iv} gives sufficiently fast convergence without causing \mathbf{K} to become too large.

Problem 13 is solved with MOSEK in YALMIP, which is feasible without numerical issues. In the solution obtained in this test, the eigenvalues of $\tilde{\mathbf{P}}_{22}\tilde{\mathbf{Q}}_{22}$ are between 0.0081 and 3.7817×10^5 , and the eigenvalues of $\text{He}\{\tilde{\mathbf{P}}^*\tilde{\mathbf{F}}_1\}$ are between -715.08 and -0.035 .

7.2 Comparing transient responses with the standard droop control

In Fig. 2, the topology of the microgrid test system is shown. The single-phase electromagnetic model of the

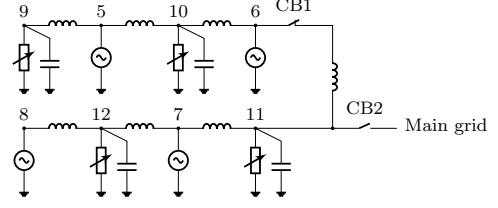


Fig. 2. Topology of the microgrid test system (ZIP loads are presented by variable resistors)

system with line dynamics is defined and numerically solved in MATLAB. At the initial condition, every bus injects or consumes the same $(1 + j0.75) \times 10^{-2}$ pu complex power before adjustment for the $R-L$ line and shunt capacitor losses. The ZIP loads are configured to have 10% constant power component at the initial condition so that they remain shifted passive if the voltage of the shunt capacitor does not drop below 0.13 pu.

Test 1. For the first test, line resistance and inductance are set to 0.2 Ω and 4 mH. The transient response of the proposed control is shown in Fig. 3a and 3b under discrete disturbances which include load changes at 0.01 and 10 s, disconnection and reconnection of the microgrid topology at 5 and 15 s, and reconnection to a stiff main grid (an infinite bus) at 20 s. The latter two are simulated as sudden actions of the circuit breakers without pre-synchronization to induce a large transient response. The frequency and voltage responses of the proposed controller in Fig. 3a and 3b are comparable to the standard droop control in Fig. 3c and Fig. 3d. We can see that the frequency and voltage responses of the proposed controller are smooth and surprisingly similar in shape. For comparison, the frequency response of the standard droop control is smooth and makes sense from the first-order dynamics of the swing equation, but the voltage response has large overshoots, which indicates that the voltage is regulated on a smaller time scale.

Test 2. The difference between the two types of control is more obvious when we change the line parameters to 0.1 Ω and 0.1 mH. These line parameters better represent a low-voltage microgrid where the distribution lines are mostly resistive. It corresponds to a decrease in the time constant of the $R-L$ line dynamics from 20 ms to 1 ms (1 kHz). The latter is on the same order of magnitude as the voltage and current loops of the standard control, which are, respectively, 0.4 and 1.6 kHz. Consistent with the analysis in [36], we can see in Fig. 4 that without changing the control gains of the standard droop control, the trajectory fails to converge after the first disturbance at 0.1 s. In comparison, the proposed controller maintains stability as the time constant of the $R-L$ lines is reduced 20 times.

The power sharing characteristic of the proposed controller under the large disturbance of the reconnection event at 20 s in the two tests is shown in Fig. 5a-d. In

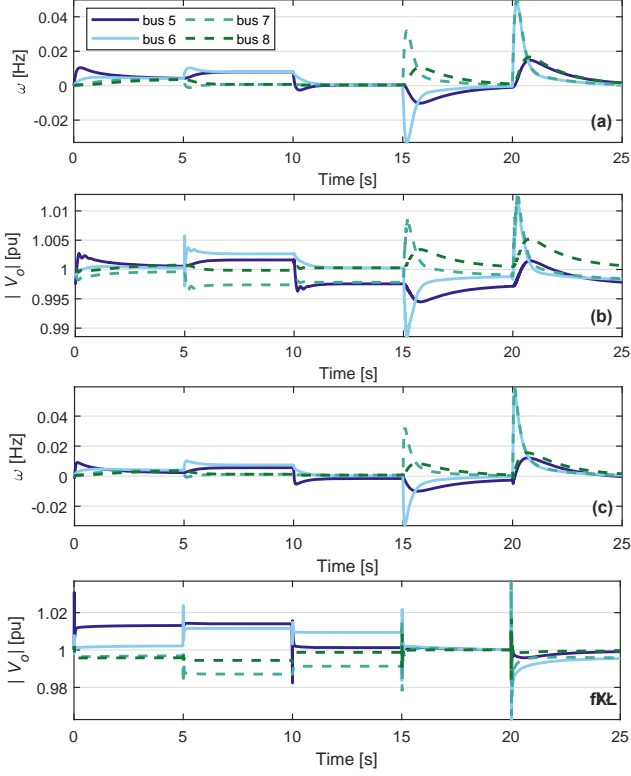


Fig. 3. Comparing the transient responses of the proposed control (a)–(b) and double-loop PI control (c)–(d) under the following disturbances: from 0.01 to 10 s, the conductance and susceptance of the Z load at Bus 9 are reduced by 40% and 50% respectively, the conductance of the Z load at Bus 10 is reduced by 20%, and the real power of the CPL at Bus 10 is increased by 40%. From 5 to 15 s, CB1 is opened. At 20 s, CB2 to the infinite bus $V_{inf} = 0.95\angle 0.6$ pu is closed

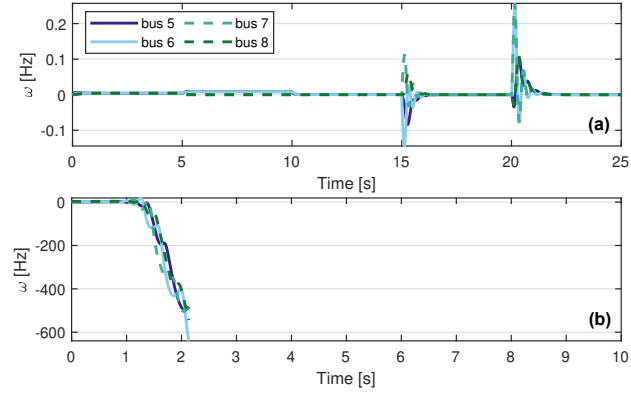


Fig. 4. Comparing the transient responses of the proposed control in (a) and baseline control in (b) with the time constant of the network R – L lines reduced from 20 ms to 1 ms.

all cases, we can see that the large power disturbances at Bus 11 are shared during the transient so that the impact on each DER is lessened. In particular, in Fig. 5, a surge of real power is injected into Bus 11 at 20 s, but the changes in DER power outputs are much milder. Comparing the power response with the two sets of line pa-

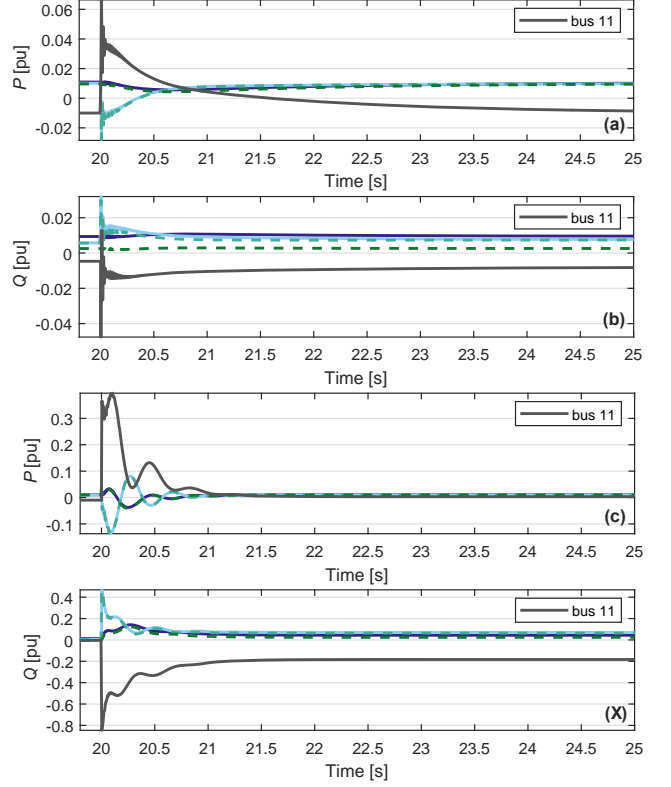


Fig. 5. Power sharing characteristic with the proposed control under reconnection to the stiff main grid without pre-synchronization, (a)–(b): time constant of R – L lines is 20 ms, (c)–(d): time constant of R – L lines is 1 ms

rameters, we can see that in Fig. 5a and 5b, the settling times of the real and reactive power are indeed much longer than in Figs. 5c and 5d, which agrees with the estimate that the response of the network in the second case is 20 times faster.

8 Conclusion

We have presented a stability proof for the non-nominal circular limit cycles of the microgrid with a general type of voltage controller at each DER generator. The hurdle of the stability proof is the reference voltage, which is an input for the voltage controller and acts as a power source for the interconnected system. Through a port-Hamiltonian model of the system with the definition of the time-varying phase $\hat{\tau}$, we formally remove the voltage sources from the energy balance equations and prove that the shifted passivity of the voltage controller, without considering the reference voltage or the swing equation, implies orbital stability. The stability condition lends itself to simpler linear control design as a semidefinite program, whose effectiveness is demonstrated through simulation, showing superior performance of the control parameters tuned based on the proposed condition versus those tuned based on time-scale separation. Improvement in control performance

includes (i) the guaranteed stability that is independent of the time constants of the distribution lines, and (ii) the uniform response in voltage and frequency such that the whole system operates on one time scale with smoother transients.

References

- [1] A. V. Bocharov, V. N. Chetverikov, S. V. Duzhin, N. G. Khorkova, I. S. Krasilshchik, A. V. Samokhin, Yu. N. Torkhov, A. M. Verbovetsky, and A. M. Vinogradov. *Symmetries and conservation laws for differential equations of mathematical physics*, volume 182. American Mathematical Society, 1999.
- [2] Nazmi Burak Budanur, Daniel Borrero-Echeverry, and Predrag Cvitanović. Periodic orbit analysis of a system with continuous symmetry—a tutorial. *Chaos: An Interdisciplinary Journal of Nonlinear Science*, 25(7), 2015.
- [3] Hsiao-Dong Chiang. *Direct methods for stability analysis of electric power systems: theoretical foundation, BCU methodologies, and applications*. John Wiley & Sons, 2011.
- [4] Claudio De Persis and Nima Monshizadeh. Bregman storage functions for microgrid control. *IEEE Transactions on Automatic Control*, 63(1):53–68, 2017.
- [5] Huagui Duan, Yiming Long, and Chaofeng Zhu. Index iteration theories for periodic orbits: old and new. *Nonlinear Analysis*, 201:111999, 2020.
- [6] Ivar Ekeland. *Convexity methods in Hamiltonian mechanics*, volume 19. Springer Science & Business Media, 2012.
- [7] Shaik Fiaz, Daniele Zonetti, Romeo Ortega, Jacquelin MA Scherpen, and AJ Van der Schaft. A port-Hamiltonian approach to power network modeling and analysis. *European Journal of Control*, 19(6):477–485, 2013.
- [8] Fulvio Forni and Rodolphe Sepulchre. Differential analysis of nonlinear systems: Revisiting the pendulum example. In *53rd IEEE Conference on Decision and Control*, pages 3848–3859. IEEE, 2014.
- [9] Gianluca Garofalo and Christian Ott. Energy based limit cycle control of elastically actuated robots. *IEEE Transactions on Automatic Control*, 62(5):2490–2497, 2016.
- [10] Dominic Groß, Catalin Arghir, and Florian Dörfler. On the steady-state behavior of a nonlinear power system model. *Automatica*, 90:248–254, 2018.
- [11] John Hauser and Chung Choo Chung. Converse Lyapunov functions for exponentially stable periodic orbits. *Systems & Control Letters*, 23(1):27–34, 1994.
- [12] Xiuqiang He, Verena Häberle, Irina Subotić, and Florian Dörfler. Nonlinear stability of complex droop control in converter-based power systems. *IEEE Control Systems Letters*, 7:1327–1332, 2023.
- [13] Jorgen K Johnsen, Florian Dorfler, and Frank Allgower. L2-gain of port-Hamiltonian systems and application to a biochemical fermenter model. In *2008 American Control Conference*, pages 153–158. IEEE, 2008.
- [14] Ramachandra Rao Kolluri, Iven Mareels, Tansu Alpcan, Marcus Brazil, Julian de Hoog, and Doreen Anne Thomas. Stability and active power sharing in droop controlled inverter interfaced microgrids: Effect of clock mismatches. *Automatica*, 93:469–475, 2018.
- [15] VV Kozlov. On the symmetry groups of dynamic systems. *Journal of Applied Mathematics and Mechanics*, 52(4):413–420, 1988.
- [16] Joseph LaSalle. Some extensions of Liapunov’s second method. *IRE Transactions on Circuit Theory*, 7(4):520–527, 1960.
- [17] Siwei Liu, Gengyin Li, and Ming Zhou. Power system transient stability analysis with integration of dfigs based on center of inertia. *CSEE Journal of Power and Energy Systems*, 2(2):20–29, 2016.
- [18] Minghui Lu. Virtual oscillator grid-forming inverters: State of the art, modeling, and stability. *IEEE Transactions on Power Electronics*, 37(10):11579–11591, 2022.
- [19] Ian R Manchester and Jean-Jacques E Slotine. Transverse contraction criteria for existence, stability, and robustness of a limit cycle. *Systems & Control Letters*, 63:32–38, 2014.
- [20] Xin Meng, Jinjun Liu, and Zeng Liu. A generalized droop control for grid-supporting inverter based on comparison between traditional droop control and virtual synchronous generator control. *IEEE Transactions on Power Electronics*, 34(6):5416–5438, 2019.
- [21] Nima Monshizadeh, Pooya Monshizadeh, Romeo Ortega, and Arjan van der Schaft. Conditions on shifted passivity of port-Hamiltonian systems. *Systems & Control Letters*, 123:55–61, 2019.
- [22] Daniel E Olivares, Ali Mehrizi-Sani, Amir H Etemadi, Claudio A Cañizares, Reza Iravani, Mehrdad Kazerani, Amir H Hajimiragha, Oriol Gomis-Bellmunt, Maryam Saeedifard, Rodrigo Palma-Behnke, et al. Trends in microgrid control. *IEEE Transactions on Smart Grid*, 5(4):1905–1919, 2014.
- [23] Colm J O’Rourke, Mohammad M Qasim, Matthew R Overlin, and James L Kirtley. A geometric interpretation of reference frames and transformations: dq0, Clarke, and Park. *IEEE Transactions on Energy Conversion*, 34(4):2070–2083, 2019.
- [24] Luís Fernando Alves Pereira and Alexandre Sanfelice Bazanella. Tuning rules for proportional resonant controllers. *IEEE Transactions on Control Systems Technology*, 23(5):2010–2017, 2015.
- [25] Lawrence Perko. *Differential Equations and Dynamical Systems*, volume 7. Springer Science & Business Media, 2013.
- [26] Nagaraju Pogaku, Milan Prodanovic, and Timothy C Green. Modeling, analysis and testing of autonomous operation of an inverter-based microgrid. *IEEE Transactions on Power Electronics*, 22(2):613–625, 2007.
- [27] Reinhold Remmert. *Theory of complex functions*, volume 122. Springer Science & Business Media, 1991.
- [28] Stefano Rivero, Fabio Sarzo, and Giancarlo Ferrari-Trecate. Plug-and-play voltage and frequency control of islanded microgrids with meshed topology. *IEEE Transactions on Smart Grid*, 6(3):1176–1184, 2014.
- [29] Clarence W Rowley, Ioannis G Kevrekidis, Jerrold E Marsden, and Kurt Lust. Reduction and reconstruction for self-similar dynamical systems. *Nonlinearity*, 16(4):1257, 2003.
- [30] Ernest K Ryu and Stephen Boyd. Primer on monotone operator methods. *Appl. comput. math.*, 15(1):3–43, 2016.
- [31] Johannes Schiffer, Denis Efimov, and Romeo Ortega. Global synchronization analysis of droop-controlled microgrids—a multivariable cell structure approach. *Automatica*, 109:108550, 2019.
- [32] Johannes Schiffer, Romeo Ortega, Alessandro Astolfi, Jörg Raisch, and Tevfik Sezi. Conditions for stability of droop-controlled inverter-based microgrids. *Automatica*, 50(10):2457–2469, 2014.

- [33] John W Simpson-Porco. Equilibrium-independent dissipativity with quadratic supply rates. *IEEE Transactions on Automatic Control*, 64(4):1440–1455, 2018.
- [34] Felix Strehle, Albertus J Malan, Stefan Krebs, and Sören Hohmann. Passivity conditions for plug-and-play operation of nonlinear static ac loads. *IFAC-PapersOnLine*, 53(2):12237–12243, 2020.
- [35] Felix Strehle, Pulkit Nahata, Albertus Johannes Malan, Sören Hohmann, and Giancarlo Ferrari-Trecate. A unified passivity-based framework for control of modular islanded ac microgrids. *IEEE Transactions on Control Systems Technology*, 30(5):1960–1976, 2021.
- [36] Irina Subotić, Dominic Groß, Marcello Colombino, and Florian Dörfler. A Lyapunov framework for nested dynamical systems on multiple time scales with application to converter-based power systems. *IEEE Transactions on Automatic Control*, 66(12):5909–5924, 2020.
- [37] Russ Tedrake. *Underactuated Robotics*. Course Notes for MIT 6.832, 2023.
- [38] Remus Teodorescu, Frede Blaabjerg, Marco Liserre, and P Chiang Loh. Proportional-resonant controllers and filters for grid-connected voltage-source converters. *IEEE Proceedings-Electric Power Applications*, 153(5):750–762, 2006.
- [39] Michele Tucci and Giancarlo Ferrari-Trecate. A scalable, line-independent control design algorithm for voltage and frequency stabilization in ac islanded microgrids. *Automatica*, 111:108577, 2020.
- [40] Arjan Van der Schaft and Dimitri Jeltsema. Port-Hamiltonian systems theory: An introductory overview. *Foundations and Trends in Systems and Control*, 1(2-3):173–378, 2014.
- [41] Xiongfei Wang, Yun Wei Li, Frede Blaabjerg, and Poh Chiang Loh. Virtual-impedance-based control for voltage-source and current-source converters. *IEEE Transactions on Power Electronics*, 30(12):7019–7037, 2014.
- [42] Frank W Warner. *Foundations of differentiable manifolds and Lie groups*, volume 94. Springer Science & Business Media, 1983.
- [43] Jeremy D Watson, Yemi Ojo, Khaled Laib, and Ioannis Lestas. A scalable control design for grid-forming inverters in microgrids. *IEEE Transactions on Smart Grid*, 12(6):4726–4739, 2021.
- [44] Bowen Yi, Romeo Ortega, Dongjun Wu, and Weidong Zhang. Orbital stabilization of nonlinear systems via mexican sombrero energy shaping and pumping-and-damping injection. *Automatica*, 112:108661, 2020.